

# Black hole triggered star formation in the dwarf galaxy Henize 2-10

Zacharay Schutte<sup>1</sup> and Amy Reines<sup>1</sup>

<sup>1</sup>*eXtreme Gravity Institute, Department of Physics, Montana State University, MT 59715, USA*

**Black hole driven outflows have been observed in some dwarf galaxies with active galactic nuclei<sup>1</sup>, and likely play a role in heating and expelling gas (thereby suppressing star formation), as they do in larger galaxies<sup>2</sup>. The extent to which black hole outflows can trigger star formation in dwarf galaxies is unclear, because work in this area has hitherto focused on massive galaxies and the observational evidence is scarce<sup>3,4,5</sup>. Henize 2-10 is a dwarf starburst galaxy previously reported to have a central massive black hole<sup>6,7,8,9</sup>, though that interpretation has been disputed since some aspects of the observational evidence are also consistent with a supernova remnant<sup>10,11</sup>. At a distance of  $\sim 9$  Mpc, it presents an opportunity to resolve the central region and determine if there is evidence for a black hole outflow impacting star formation. Here we report optical observations of Henize 2-10 with a linear resolution of a few parsecs. We find a  $\sim 150$  pc long ionized filament connecting the region of the black hole with a site of recent star formation. Spectroscopy reveals a sinusoid-like position-velocity structure that is well described by a simple precessing bipolar outflow. We conclude that this black hole outflow triggered the star formation.**

Radio observations of Henize 2-10 using very long baseline interferometry reveal a nuclear, compact, non-thermal source with a luminosity of  $L_R \sim 4 \times 10^{35}$  erg s<sup>-1</sup> and a physical size

$< 3 \text{ pc} \times 1 \text{ pc}$ <sup>7</sup>. High-resolution X-ray observations unveil a point source with  $L_x \sim 10^{38} \text{ erg s}^{-1}$  that is spatially coincident with the compact nuclear radio source<sup>8</sup>. There are two possible explanations for these radio and X-ray observations alone - a highly sub-Eddington massive black hole (i.e., a low-luminosity AGN) or a very young supernova remnant<sup>7,10</sup>. However, there are other observational results to consider regarding the origin of the nuclear radio/X-ray source in Henize 2-10. We summarize these results in Table 1 (Methods) and demonstrate that a highly sub-Eddington massive black hole is consistent with all of the available observations including new results presented here, while a supernova remnant is not.

We observed Henize 2-10 at optical wavelengths using the Space Telescope Imaging Spectrograph (STIS) on the *Hubble Space Telescope (HST)*. We obtained observations of the central regions of Henize 2-10 with the 0.2"-slit in two orientations. The first, referred to as the EW orientation, is centered on the nuclear radio/X-ray source and aligned with the filamentary ionized structure between the two bright, extended regions of ionized gas previously identified in narrowband  $H\alpha$  imaging with *HST*<sup>6</sup> (Figure 1). The second, referred to as the NS orientation, is centered on the nuclear source and rotated  $90^\circ$  with respect to the EW observation. We obtained high-dispersion observations (velocity resolution of  $\sim 40 \text{ km s}^{-1}$ ) at both slit positions using the G750M and G430M gratings, which cover the strong emission lines of interest (e.g.,  $H\alpha$ , [NII], [SII], [OI] and  $H\beta$ , [OIII], respectively).

The kinematics of the ionized gas provide evidence for an outflow originating from a nuclear massive black hole. First, we detect significantly broadened emission lines at the location of the central source in both slit orientations. In particular, the [OI]6300 emission

line has a broad component with a full width at half maximum (FWHM) of  $497 \text{ km s}^{-1}$  as measured in the EW slit (and  $445 \text{ km s}^{-1}$  in the NS slit) using a 3-pixel extraction region in the spatial dimension. While the [OI] line is too weak to be detected all along the EW filament (or NS slit), it is detected at the location of the bright star-forming region  $\sim 70 \text{ pc}$  to the east with a FWHM =  $103 \text{ km s}^{-1}$ , much less than that of the central source (e.g., see top left panel of Figure 2). The [OIII]5007 line is much stronger than [OI]6300 and detectable all along the EW filament. The FWHM of the broad component of [OIII] at the location of the nuclear source is  $271 \text{ km s}^{-1}$ , which is somewhat broader than the median value per spatial pixel along the EW slit ( $175 \text{ km s}^{-1}$  with a standard deviation of  $53 \text{ km s}^{-1}$ ). We do not observe such broad emission beyond the location of the central source in the NS slit (see top right panel of Figure 2). We emphasize that the line widths at the location of the nuclear source are consistent with a low-velocity outflow from a massive black hole, but would be anomalously low for a very young supernova remnant with typical FWHMs of thousands of  $\text{km s}^{-1}$  <sup>13,14</sup>.

In addition to broadened emission lines at the location of the central source, we also find Doppler shifted velocities along the EW slit that exhibit a coherent sinusoid-like pattern that is relatively smooth, especially in comparison to the position-velocity diagram along the NS slit orientation that shows no evidence of a coherent pattern in the Doppler velocities of strong emission lines (see Figure 2 and Methods). Moreover, a simple model of a precessing bipolar outflow broadly reproduces the observed sinusoid-like velocity pattern along the EW slit that is aligned with the ionized filament seen in narrowband  $\text{H}\alpha$  imaging with HST (see Methods for a description of the model). Precessing jets have been observed in many AGNs, although they are typically found in more luminous quasars and

radio galaxies<sup>15,16</sup>. Theories for the origin of precessing jets/outflows include accretion disk warping, jet instabilities, and the presence of massive black hole binaries<sup>17,18</sup>. On the other hand, the coherent velocity pattern we observe over  $\sim 150$  pc along the ionized filament centered on the central source is incompatible with a supernova remnant origin since supernova remnants do not drive quasi-linear outflows on such large scales.

There is also evidence that the black hole outflow is triggering the formation of star clusters in the central region of Henize 2-10. *HST* imaging shows that the ionized filament extends eastward from the massive black hole to a bright knot of ionized gas and site of recent star formation located  $1.5''$  ( $\sim 70$  pc) away from the black hole (Figure 3). Given that our *HST* spectroscopy along this filament exhibits a continuous velocity pattern, which can be tracked from the black hole to the eastern star-forming region and is well described by a precessing bipolar outflow model, this strongly suggests that the outflow driven by the black hole is causally connected to the region of recent star formation. There is also a secondary, blue-shifted peak (offset by  $154 \text{ km s}^{-1}$ ) detected in the emission lines at the location of the bright star-forming knot, suggesting the outflow is pushing the line-emitting gas clouds and influencing their kinematics (Figure 3). The double peaked lines would naturally arise as the outflow intercepted dense gas and primarily pushed it in the lateral direction rather than ahead of the flow. The handful of young star clusters associated with the star-forming knot have ages of  $\sim 4$  Myr (see Methods) and are predominately aligned in the north-south direction, consistent with a scenario in which they formed from gas moving in opposite directions due to the impact of the black hole outflow<sup>19</sup>. There is also a local peak in the gas density at the location of the star-forming knot with  $n_e \gtrsim 10^4 \text{ cm}^{-3}$  (see Figure 6 in Methods), consistent with the outflow compressing gas clouds and

enhancing star formation in this region. It is notable that we also detect double peaked emission line profiles to the west of the massive black hole at the boundary of a dark cloud of gas and dust (region 5, see Figure 7 in Methods), suggesting the other side of the bipolar outflow is also intercepting dense clouds and pushing them perpendicular to the outflow direction. Just to the west of this region (region 6, Figure 7 in Methods), the equivalent width of the  $H\alpha$  emission line indicates stellar ages  $\lesssim 3$  Myr, indicating a very early stage of star formation in which the infant star clusters have not had enough time to destroy or disperse the dense molecular gas from which they formed, leading to high levels of extinction<sup>20</sup>.

The ionization conditions of the gas provide additional support for a massive black hole with an outflow. First, our *HST* spectroscopy at  $\sim 0.1''$  resolution clearly reveals non-stellar ionization at the location of the central source based on the flux ratio of  $[OI]/H\alpha$ , which is consistent with gas photoionized by an accreting massive black hole (Figure 8 in Methods). Additionally, supernova remnants are known to be strong  $[SII]$  emitters with  $\log [SII]/H\alpha > -0.5$ <sup>21</sup>, which is not seen in the STIS spectrum of the nuclear source. The ionization conditions probed by optical diagnostics using  $[OIII]/H\beta$  versus  $[NII]/H\alpha$  and  $[SII]/H\alpha$  do not clearly indicate a (luminous) AGN, which at first glance may seemingly rule out the presence of a massive black hole. However, there are a number of potential reasons for this apparent discrepancy. First,  $[NII]$  and  $[SII]$  are not as sensitive to the hardness of the ionizing radiation field as  $[OI]$  and are therefore less reliable at identifying AGNs. Second, the massive black hole in Henize 2-10 is accreting at a tiny fraction of its Eddington luminosity ( $\sim 10^{-6} L_{\text{Edd}}$ )<sup>6</sup>, which can impact emission lines such that they do not look like those of luminous AGNs with higher Eddington ratios<sup>22</sup>. The apparent contradiction of

emission line diagnostics can also arise when there is underlying star formation contributing to the spectrum. Finally, we note that there are other examples of radio-selected massive black holes in dwarf galaxies with enhanced [OI] that do not look like optical AGNs in the other diagnostic diagrams<sup>23,24</sup>.

We also find that the ionization conditions probed by strong emission line ratios at the location of the central source and along the filament are well described by theoretical models of shocks propagating in a high density medium<sup>25</sup> (see Methods). Specifically, emission line ratios in the central  $\sim 150$  pc along the EW slit orientation are consistent with models of a shock with a velocity of  $\sim 200$  km s<sup>-1</sup> traveling through a gas with an electron density of  $\sim 1000$  cm<sup>-3</sup> and include a ‘precursor’ of ionizing photons that travel upstream from the shock front pre-ionizing the gas. The model shock velocities that match the strong emission line ratios agree with those obtained from direct measurements of the line widths from our kinematic study described above (e.g., [OIII]), and the model gas densities are consistent with our measurements using the density sensitive line ratio [SII]6716/6731 (see Methods). Moreover, these conditions are well explained by an AGN-driven outflow mechanically exciting the interstellar medium in these regions in addition to the precursor component contributing to the photoionization of the interstellar medium. There is also evidence for shocked emission at the location of the eastern star-forming region, particularly from the secondary blue-shifted peak, in addition to photoionization from young hot stars (see Methods). Combining these results with our kinematic study indicates that the bipolar outflow generated by the central black hole is shocking the interstellar medium in the central regions of Henize 2-10, creating conditions that are favorable for positive AGN feedback<sup>26,27</sup>.

AGN driven outflows have been discovered in a small sample of dwarf galaxies, though the discovery of a black hole outflow in Henize 2-10 provides the first example that is robustly spatially resolved. Moreover, Henize 2-10 differs from these other systems in several other ways. The majority of black hole driven outflows in dwarf galaxies have been found in galaxies with well-defined nuclei and optically-selected AGNs with relatively high accretion rates. These observations suggest the AGNs play a role in heating and expelling gas in the galaxies and quenching star formation, a phenomenon known as negative feedback<sup>28</sup>. This is in stark contrast with Henize 2-10, which has an irregular central morphology, is intensely forming stars, and is experiencing positive feedback from a weakly accreting black hole that is luminous at radio, rather than optical, wavelengths.

Indeed, “jet-mode” feedback is often associated with radio-loud AGNs accreting at low Eddington ratios, and attributed to the unbound nature of radiatively inefficient accretion flows<sup>29,30</sup>. Warm ionized gas outflows are observed to accompany the radio jets/outflows in some cases, particularly in young radio galaxies where nascent jets are expanding through the interstellar medium in the central regions of their hosts<sup>30</sup>. In these systems, the spatial extents of the warm outflows (traced by emission lines) are similar to the radio morphologies. A similar phenomenon is observed in Henize 2-10, which is most readily seen in a comparison between the radio emission detected with the Very Large Array and Pa $\alpha$  emission detected by *HST* in the central few hundred pc of the galaxy<sup>4</sup>. However, an important difference between Henize 2-10 and powerful young radio galaxies is that the emission lines are dominated by AGN photoionization in the more massive and luminous systems, whereas the extended emission line regions in Henize 2-10 are dominated by star

formation (enhanced/triggered by the black hole outflow). Therefore, Henize 2-10 may be a low-mass, low-power analog of young radio galaxies.

1. Manzano-King, Christina M., Gabriela Canalizo, and Laura V. Sales. AGN-Driven Outflows in Dwarf Galaxies. *The Astrophysical Journal* 884.1 (2019): 54.
2. Fabian, Andrew C. "Observational evidence of active galactic nuclei feedback." *Annual Review of Astronomy and Astrophysics* 50 (2012): 455-489. Reines, Amy E., et al. "An actively accreting massive black hole in the dwarf starburst galaxy Henize 2-10." *Nature* 470.7332 (2011): 66-68.
3. Gaibler, Volker, et al. "Jet-induced star formation in gas-rich galaxies." *Monthly Notices of the Royal Astronomical Society* 425.1 (2012): 438-449.
4. Maiolino, Roberto, et al. "Star formation inside a galactic outflow." *Nature* 544.7649 (2017): 202-206.
5. Gallagher, Robert, et al. "Widespread star formation inside galactic outflows." *Monthly Notices of the Royal Astronomical Society* 485.3 (2019): 3409-3429.
6. Reines, Amy E., et al. "An actively accreting massive black hole in the dwarf starburst galaxy Henize 2-10." *Nature* 470.7332 (2011): 66-68.
7. Reines, Amy E., and Adam T. Deller. "Parsec-scale radio emission from the low-luminosity active galactic nucleus in the dwarf starburst galaxy Henize 2-10." *The Astrophysical Journal Letters* 750.1 (2012): L24.
8. Reines, Amy E., et al. "Deep Chandra observations of the compact starburst galaxy Henize 2–10: X-rays from the massive black hole." *The Astrophysical Journal Letters* 830.2 (2016): L35.
9. Riffel, Rogemar A. "Evidence for an accreting massive black hole in He 2–10 from adaptive optics integral field spectroscopy." *Monthly Notices of the Royal Astronomical Society* 494.2 (2020): 2004-2011.

10. Hebbar, Pavan R., et al. "X-ray spectroscopy of the candidate AGNs in Henize 2–10 and NGC 4178: likely supernova remnants." *Monthly Notices of the Royal Astronomical Society* 485.4 (2019): 5604-5615.
11. Cresci, Giovanni, et al. "The MUSE view of He 2-10: No AGN ionization but a sparkling starburst." *Astronomy & Astrophysics* 604 (2017): A101.
12. Kobulnicky, Henry A., et al. "Aperture Synthesis Observations of Molecular and Atomic Gas in the Wolf-Rayet Starburst Galaxy." *The Astronomical Journal* 110 (1995): 116.
13. Mathewson, D. S., et al. "A new oxygen-rich supernova remnant in the Large Magellanic Cloud." *The Astrophysical Journal* 242 (1980): L73-L76.
14. Borkowski, Kazimierz J., et al. "Asymmetric Expansion of the Youngest Galactic Supernova Remnant G1. 9+ 0.3." *The Astrophysical Journal Letters* 837.1 (2017): L7.
15. Gower, A. C., and J. B. Hutchings. "A precessing relativistic jet model for 3C 449." *The Astrophysical Journal* 258 (1982): L63-L66.
16. Dunn, R. J. H., A. C. Fabian, and J. S. Sanders. "Precession of the super-massive black hole in NGC 1275 (3C 84)?" *Monthly Notices of the Royal Astronomical Society* 366.3 (2006): 758-766.
17. Pringle, J. E. "Self-induced warping of accretion discs." *Monthly Notices of the Royal Astronomical Society* 281.1 (1996): 357-361.
18. Nixon, Chris, and Andrew King. "Do jets precess... or even move at all?." *The Astrophysical Journal Letters* 765.1 (2013): L7.
19. Kharb, P., et al. "Double-peaked Emission Lines Due to a Radio Outflow in KISSR 1219." *The Astrophysical Journal* 846.1 (2017): 12.
20. Beck, Sara C., Jean L. Turner, and S. Michelle Consiglio. "Dense Molecular Filaments Feeding a Starburst: ALMA Maps of CO (3–2) in Henize 2–10." *The Astrophysical Journal* 867.2 (2018): 165.

21. Lee, Myung Gyoon., et al. "Optical Spectroscopy of Supernova Remnants in M81 and M82." *The Astrophysical Journal* 804.1 (2015): 63.
22. Trump, Jonathan R., et al. "Accretion Rate and the Physical Nature of Unobscured Active Galaxies." *The Astrophysical Journal* 733.1 (2011): 60.
23. Reines, Amy E., et al. "A new sample of (wandering) massive black holes in dwarf galaxies from high-resolution radio observations." *The Astrophysical Journal* 888.1 (2020): 36.
24. Molina, Mallory, et al. "Outflows, Shocks, and Coronal Line Emission in a Radio-selected AGN in a Dwarf Galaxy." *The Astrophysical Journal* 910.1 (2021): 5.
25. Allen, Mark G., et al. "The MAPPINGS III library of fast radiative shock models." *The Astrophysical Journal Supplement Series* 178.1 (2008): 20.
26. Silk, Joseph, and Colin Norman. "Global star formation revisited." *The Astrophysical Journal* 700.1 (2009): 262.
27. Silk, Joseph. "Unleashing positive feedback: linking the rates of star formation, supermassive black hole accretion, and outflows in distant galaxies." *The Astrophysical Journal* 772.2 (2013): 112.
28. Penny, Samantha J., et al. "SDSS-IV MaNGA: evidence of the importance of AGN feedback in low-mass galaxies." *Monthly Notices of the Royal Astronomical Society* 476.1 (2018): 979-998.
29. Trump, Jonathan R., et al. "Spectropolarimetric evidence for radiatively inefficient accretion in an optically dull active galaxy." *The Astrophysical Journal* 732.1 (2011): 23.
30. Santoro, F., et al. "AGN-driven outflows and the AGN feedback efficiency in young radio galaxies." *Astronomy & Astrophysics* 644 (2020): A54.

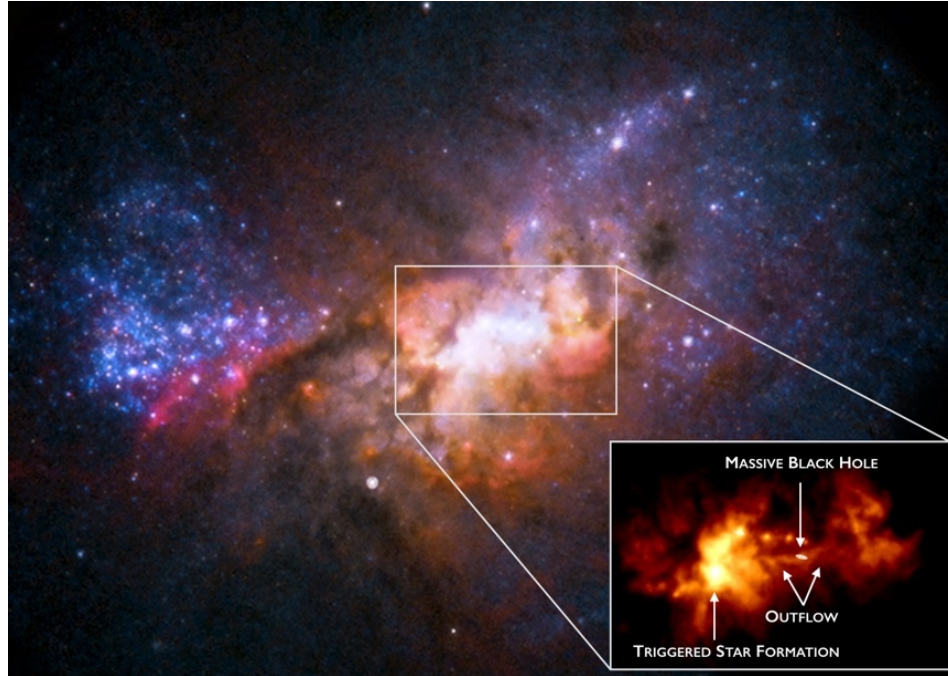


*Figure 1: HST optical image of the dwarf starburst galaxy Henize 2-10 (Image credit: NASA/STScI). The inset shows a narrowband H $\alpha$ +continuum image of the central 6" x 4" region. At the distance of Henize 2-10 ( $\sim 9$  Mpc), 1" corresponds to  $\sim 44$  pc. White contours indicate compact radio emission detected with very long baseline interferometry and mark the location of the central massive black hole<sup>7</sup>, which is also detected in X-rays<sup>8</sup>. Our HST spectroscopy demonstrates that the black hole is driving an outflow that is triggering the formation of young massive star clusters. The main image is 25" ( $\sim 1.1$  kpc) across.*

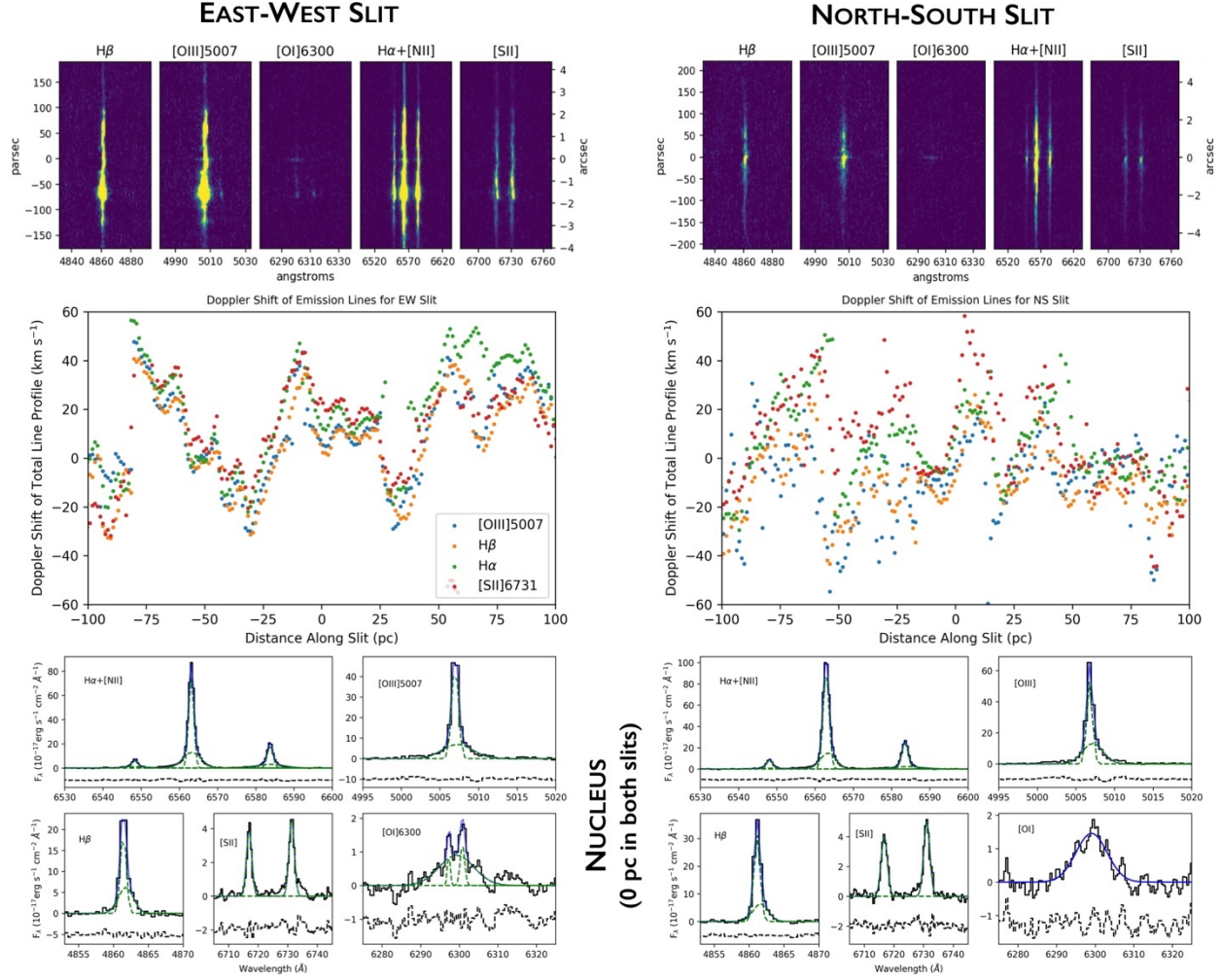


Figure 2: Top panels show 2D continuum-subtracted *HST* STIS spectra of key emission line regions along the EW and NS slit orientations. The middle panels show position-velocity diagrams along each slit position where Doppler shifts are relative to the systemic velocity of the galaxy ( $873 \text{ km s}^{-1}$ )<sup>12</sup>. The velocity pattern in the EW slit is much more coherent than that in the NS slit. The bottom panels show extracted 1D spectra at the location of the nuclear massive black hole. The region surrounding the nucleus (0 pc in both slit positions) shows strong broadened emission lines, including [O]6300 and [OIII]5007.

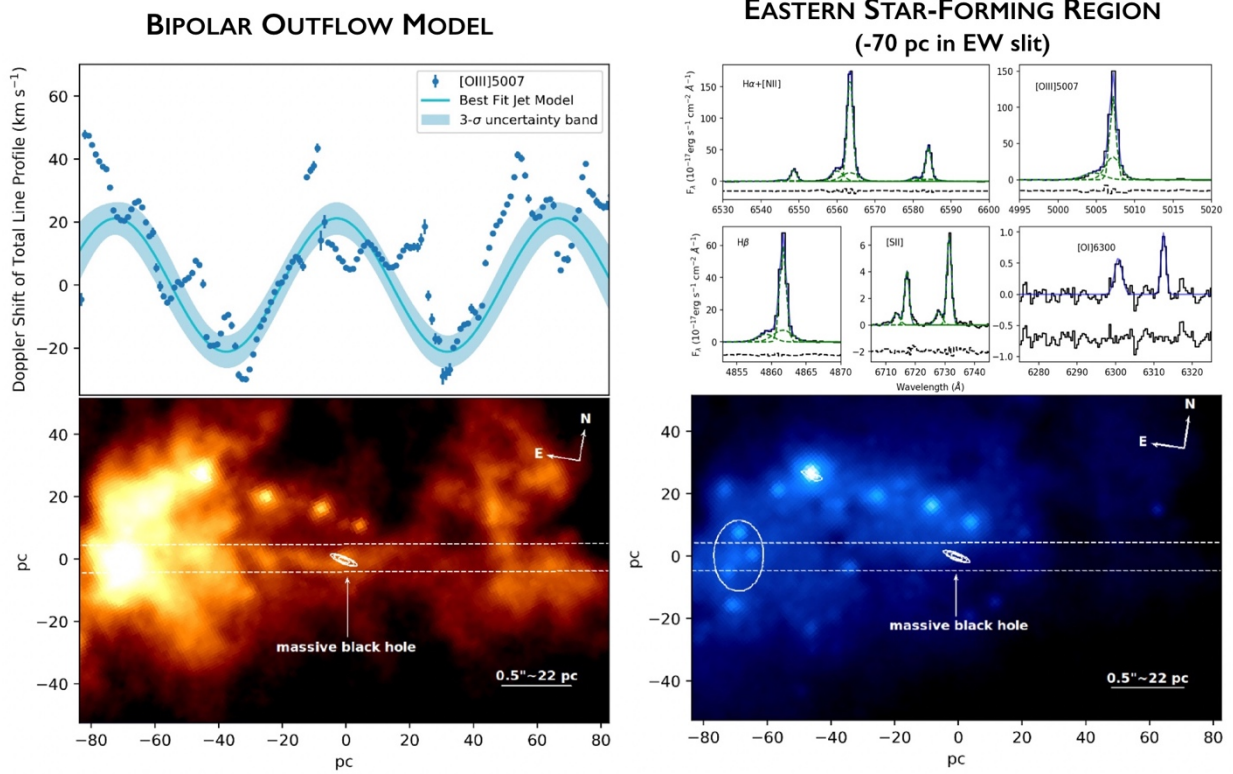


Figure 3: Top left: Position-velocity diagram of the  $[OIII]5007$  emission line along the EW slit where the Doppler shifts are relative to the systemic velocity of the galaxy ( $873 \text{ km s}^{-1}$ )<sup>12</sup>. The data are well described by a simple precessing outflow model with a precession frequency of  $f \sim 5 \text{ revolutions Myr}^{-1}$  and a precession angle of  $\theta \sim 4^\circ$  (see Methods). Bottom left: HST narrowband  $H\alpha$ +continuum image showing that the EW slit position is aligned with the ionized filamentary structure connecting the massive black hole and site of recent star formation  $\sim 70 \text{ pc}$  to the east. White contours indicate compact radio emission from very long baseline interferometry<sup>7</sup>, and show the location of the massive black hole. Bottom right: HST 0.8 micron ( $\sim I$ -band) broadband image with the same field of view. Young star clusters in the eastern star-forming region are highlighted with an ellipse. Top right: Spectra of the eastern star-forming region ( $\sim 70 \text{ pc}$ ) show strong broad emission lines with a secondary blue shifted peak most clearly visible in the  $[SII]$  emission.

## Methods

### The Controversy – Massive Black Hole or Supernova Remnant

In recent years, evidence has been mounting for a massive black hole powering a low-luminosity active galactic nucleus (AGN) at the center of Henize 2-10<sup>6,7,8,9</sup>, although a supernova remnant has been proposed as an alternative by some authors<sup>10,11</sup>. As discussed in the main text, the radio and X-ray point source luminosities are consistent with both. A recent study<sup>10</sup> argues for a supernova remnant based on their findings that the X-ray spectrum is better fit by a hot plasma model (typically used for supernova remnants) than a power-law model (typically used for luminous AGNs). However, the soft X-ray spectrum of the nuclear source in Henize 2-10 does resemble massive black holes accreting at very low Eddington fractions<sup>31</sup> including Sagittarius A\* in the Milky Way<sup>32</sup>. Another study using ground-based spectroscopy favored a supernova remnant origin for the central source based on a lack of any AGN ionization signatures<sup>11</sup>. However, the ground-based observations used in that work had an angular resolution of  $\sim 0.7''$ , which is not sufficient to cleanly isolate the weakly accreting black hole from nearby young ( $< 5$  Myr) massive ( $M_{\star} \sim 10^5 M_{\odot}$ ) star clusters that dominate the line ratios at this relatively coarse angular resolution.

There are other observational results to consider regarding the origin of the nuclear radio/X-ray source in Henize 2-10. For example, a recent study using adaptive optics integral field spectroscopy provides evidence for gas excited by an AGN and an enhanced stellar velocity dispersion at the location of the nuclear source consistent with a  $\sim 10^6 M_{\odot}$  black hole, favoring the low-luminosity AGN interpretation<sup>9</sup>. There is also evidence for moderately significant variability on hour-long timescales in the X-ray light curve, which is

incompatible with a supernova remnant<sup>8,10</sup>. Moreover, it is reasonable to expect that Henize 2-10 hosts a massive black hole since its overall structure resembles an early-type galaxy (albeit with a central starburst) and its stellar mass may be as high as  $M_{\star} \sim 10^{10} M_{\odot}$ <sup>33</sup>, a regime where the black hole occupation fraction is near unity<sup>34</sup>. The central starburst complicates the identification of the weakly accreting black hole, yet a variety of multiwavelength observational results taken collectively strongly support its presence. These results are summarized in Table 1. A highly sub-Eddington massive black hole is

Observations	Consistent with massive black hole?	Consistent with supernova remnant?	Notes and References
Nuclear, non-thermal radio point source with $L_R \sim 4 \times 10^{35}$ erg/s	yes	yes	<ul style="list-style-type: none"> <li>Nuclear, non-thermal point source detected with the VLA (Johnson et al. 2003; Reines et al. 2011).</li> <li>VLBI observations confirm non-thermal origin and constrain the nuclear radio source to be <math>\lesssim 3 \times 1</math> pc. If SNR, size and luminosity imply it must be very young (Reines &amp; Deller 2012).</li> </ul>
Spatially coincident nuclear X-ray point source with $L_X \sim 10^{38}$ erg/s	yes	yes	<ul style="list-style-type: none"> <li>Nuclear X-ray point source detected with <i>Chandra</i> that is spatially coincident with radio source. If massive BH, X-ray luminosity implies highly sub-Eddington accretion, which is consistent with soft X-ray spectrum. An X-ray binary is ruled out by the high luminosity of the compact radio source (Reines et al. 2016).</li> <li>X-ray spectrum also consistent with SNR (Hebbar et al. 2019)</li> </ul>
X-ray variability on hr-long timescales	yes	no	<ul style="list-style-type: none"> <li>X-ray light curve from 160 ks <i>Chandra</i> observation exhibits moderately significant variability (a factor of <math>\sim 2</math>; Reines et al. 2016). Probability of non-variable light curve producing the signal is 3% (Hebbar et al. 2019).</li> <li>Tentative detection of <math>\sim 9</math>-hr periodicity in the variable light curve (Reines et al. 2016).</li> </ul>
Enhanced stellar velocity dispersion at location of nuclear source	yes	no	<ul style="list-style-type: none"> <li>Stellar velocity dispersion map from near-IR IFU observations reveals enhancement of <math>\sim 7</math> km/s at position of nuclear source, consistent with a BH mass of <math>\sim 1.5 \times 10^6 M_{\text{sun}}</math> (Riffel et al. 2020). This is in line with expectations given the stellar mass of Henize 2-10 (<math>\sim 10^{10} M_{\text{sun}}</math>; Nguyen et al. 2014).</li> <li>No detectable star cluster at location of the central source (Reines et al. 2011). This is in contrast to a weaker, more extended off-nuclear VLBI source, which is co-spatial with the most luminous super star cluster in Henize 2-10, and is a likely SNR (Reines &amp; Deller 2012).</li> </ul>
Gas excitation and ionization conditions	yes	?	<ul style="list-style-type: none"> <li>Enhanced near-IR [Fe II]/Br<math>\gamma</math> ratio consistent with accreting BH or supernova driven shocks (Riffel et al. 2020; Cresci et al. 2010).</li> <li>Near-IR H<math>\alpha</math> line ratios consistent with AGN photoionization (Riffel et al. 2020).</li> <li>Optical line ratios from ground-based spectra dominated by star formation (Cresci et al. 2017).</li> <li>HST/STIS observations show non-stellar emission-line ratios involving [O]. SNRs have <math>\log [SII]/H\alpha &gt; -0.5</math>, which is not seen in the STIS spectrum of the nuclear source (<b>this work</b>).</li> </ul>
Gas kinematics and morphology	yes	no	<ul style="list-style-type: none"> <li>Spectroscopy at high spatial resolution shows broadened near-IR and optical emission lines at the location of the central source (Riffel et al. 2020 and <b>this work</b>). In particular, [OII]6300 has a FWHM of <math>\sim 500</math> km/s indicating an outflow from the central source (<b>this work</b>). Very young SNRs typically have broad lines with widths on the order of thousands of km/s.</li> <li>HST/STIS spectroscopy along a <math>\sim 150</math> pc-long ionized gas filament centered on the nuclear source (seen in H<math>\alpha</math> imaging with HST) exhibits a coherent sinusoid-like pattern in the Doppler shifted velocities. The position-velocity data is well-fit by a simple model of a precessing bipolar outflow from a massive BH, and is incompatible with a SNR (<b>this work</b>).</li> </ul>

*Table 1: Summary of observational results regarding the nature of the nucleus in Henize 2-10. A highly sub-Eddington massive black hole is consistent with all of the available observations including new results presented here, while a supernova remnant is not.*

consistent with all of the observations, including the new work presented here, while a supernova remnant is not. The present study not only adds to the evidence for a massive black hole in Henize 2-10, it also demonstrates that a bipolar outflow from the black hole is enhancing/triggering star formation in its vicinity.

### **STIS Observations and Data Reduction**

Spatially resolved spectroscopic observations of the nuclear regions of the dwarf starburst galaxy Henize 2-10 were obtained using the Space Telescope Imaging Spectrograph (STIS) instrument on the *Hubble Space Telescope (HST)*. We obtained observations with two slit orientations. The first is aligned with the quasi-linear ionized gas structure identified by Reines et al.<sup>6</sup> and covers the central radio/X-ray source and the bright knot of ionized gas to the east. We refer to this as the East-West (EW) orientation. The second slit orientation was placed perpendicular to the EW observation at the location of the central radio/X-ray source. We refer to this as the North-South (NS) orientation. The candidate AGN itself was too faint to acquire directly, therefore we used a target acquisition with an offset from a bright point source 7.9" to the southeast.

Spectra were taken with the G750M and G430M gratings providing medium spectral resolution ( $R \sim 5000 - 6000$ ) coverage of key optical emission lines. The central wavelengths were set at 6581 Å and 4961 Å for the G750M and G430M gratings, respectively. At each slit orientation, two orbits were spent in G430M and one orbit in G750M. The observations were taken with a two-point dither pattern with CR-SPLITS at each position to help eliminate cosmic rays. The calibrated dithered images were combined and have a spatial resolution of  $\sim 0.1''$ , which corresponds to a physical scale of  $\sim 4$  pc at the distance of Henize 2-10 ( $\sim 9$  Mpc).

## Emission Line Fitting

Before we fit emission lines in the spectra, we first modeled and removed the continuum. The reduced spectra were continuum-subtracted by masking emission line regions and fitting a low order polynomial to the continuum in each row in the spatial dimension. A low order polynomial was used given the lack of absorption features in the spectra. We did, however, consider the potential impact of stellar absorption lines on our measurements and found that the absorption line strengths are negligible compared to the emission line strengths. Scaling a Starburst99<sup>35</sup> model for a 4 Myr stellar population (see Stellar Ages section below) to our observed spectra, we find that the flux of  $H\alpha$  absorption is smaller by a factor of 61 than the  $H\alpha$  emission and the flux of the  $H\beta$  absorption is smaller by a factor of 7 than the  $H\beta$  emission at the location of the central source. Accounting for this absorption has a negligible effect on the line ratios of the nuclear source and does not impact the classifications based on the diagnostic diagrams.

Once the spectra were continuum-subtracted, we fit each emission line of interest with a linear combination of Gaussian profiles to characterize the flux and estimate kinematic properties along the spatial dimension of each slit. The fitting was done using `lmfit`<sup>36</sup>, a non-linear least squares curve fitting package in Python. We fit each emission line with up to two Gaussian components when needed. To determine if a second Gaussian component is warranted, we require that the flux of both components be greater than the  $3\sigma$  error of the flux. This process is performed row by row in the spatial direction along each slit for emission lines of interest. During this process we fit the  $H\beta$ , [OIII]5007,  $H\alpha$ , [NII]6548/6583 and [SII]6716/6731 emission lines. We fit the  $H\alpha$  and [NII] lines simultaneously, fixing the spacing between [NII] Gaussian components to their

corresponding component in the  $H\alpha$  emission line to laboratory values. Additionally, we tie the widths of [NII] components and fix the flux ratio of the [NII] lines to the laboratory value of 1:2.96. Similarly, the two [SII] emission lines are fit simultaneously with the spacing between Gaussian components of the two lines held fixed and the widths of the Gaussian components are tied together.

We also fit [OI]6300 in the spectra of the nuclear source and the eastern star-forming region, but the line is too weak to be detected all along the slits. Since the [OI]6300 line has a complex profile at the location of the black hole, with possible double peaked narrow lines and a much broader component than the other emission lines, we confirmed that this was not due to an artifact in the data. In Figure 4, we show close-up views of the raw 2D spectra along the EW slit position. The two images correspond to the two dithered sub-

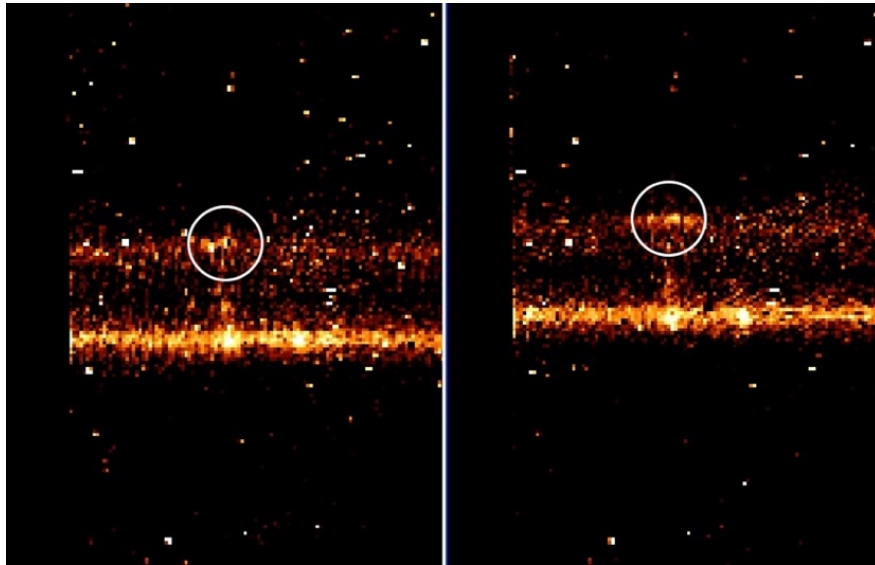


*Figure 4: Raw 2D spectra showing the [OI]6300 emission line at the location of the nucleus (indicated by white circles) in the EW slit orientation. The two images correspond to the two dithered sub-exposures.*

exposures offset by 7.5 pixels. The broad [OI] line at the location of the central source is seen in both images at different positions on the detector (indicated by white circles). Note that the locations of hot pixels do not change between the two images. Below, we also show the final reduced 2D image with the sub-exposures combined. The broad, double peaked nature of the [OI] line is clearly visible. We also note that [OI] is similarly broadened in the nuclear spectrum extracted from the NS slit position, although there is not an obvious double-peaked narrow line component (see Figure 2 in the main paper). In any case, broadened [OI] is clearly detected at the location of the nuclear source in both slit positions indicating an outflow on the order of  $\sim 500 \text{ km s}^{-1}$ .

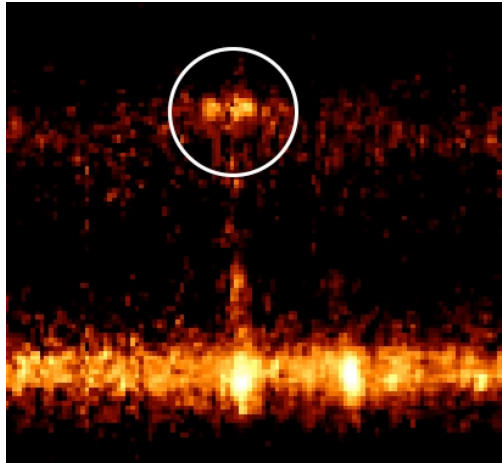


*Figure 5: Same as Figure 4 but showing the reduced 2D image with the sub-exposures combined.*

### **Gas Density**

We estimate the electron density,  $n_e$ , using the density sensitive line ratio

[SII]6716/6731<sup>37</sup>. This ratio is sensitive to electron densities in the range of  $\sim 10^2 - 10^4$

$\text{cm}^{-3}$ . Along the EW slit orientation, we find a range of  $n_e \sim 10^{2.5} - 10^4 \text{ cm}^{-3}$ , indicating a

relatively high-density gas (see Figure 6). These density estimates are in general agreement

with the gas densities predicted by the Allen et al.<sup>25</sup> shock/shock+precursor models in the central regions of Henize 2-10 as described in the next section.

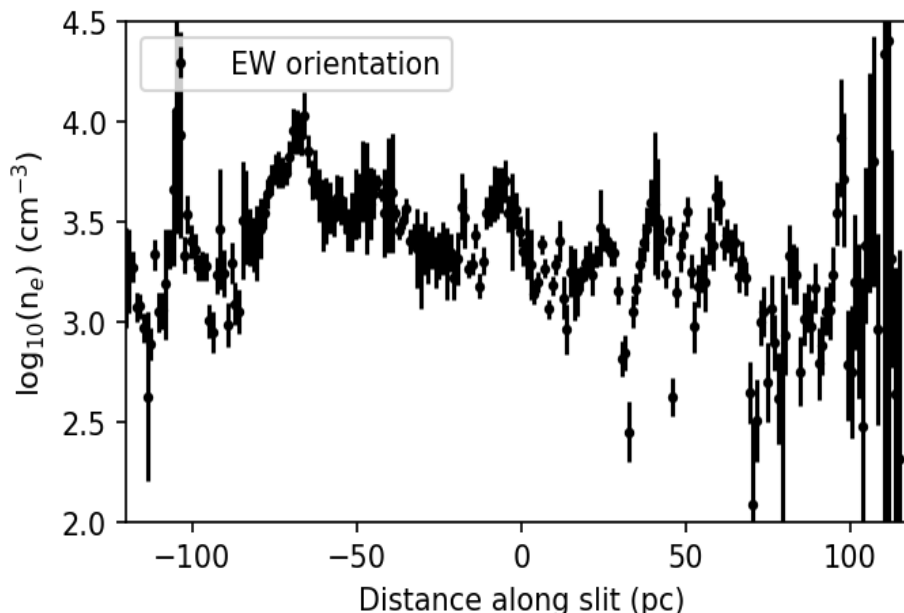


Figure 6: The electron density,  $n_e$ , measured from the ratio of  $[SII]6716/[SII]6731$  along the EW slit orientation. We find the electron density ranges from  $\sim 10^{2.5} - 10^4$ , which is within the range the  $[SII]$  ratio is sensitive to density. The high densities are consistent with those predicted by optical emission line diagnostics derived from the Allen et al.<sup>25</sup> shock models.

### Emission Line Diagnostics - Photoionization and Shock Models

To understand the ionization mechanisms in the central regions of Henize 2-10 we compare our emission line measurements in various regions to photoionization and shock models. In addition to the central radio/X-ray source, we identified 7 regions of interest that are shown in Figure 7 and serve to provide a spatially resolved picture of the kinematics and ionization conditions in the central regions of Henize 2-10. The extraction regions taken along the EW slit orientation were chosen to correspond with emission features seen in the  $H\alpha$  and  $I$ -band imaging from *HST* (young star clusters, knots of ionized gas) as well as features seen in the *STIS* spectroscopy (broad emission, double peaks).

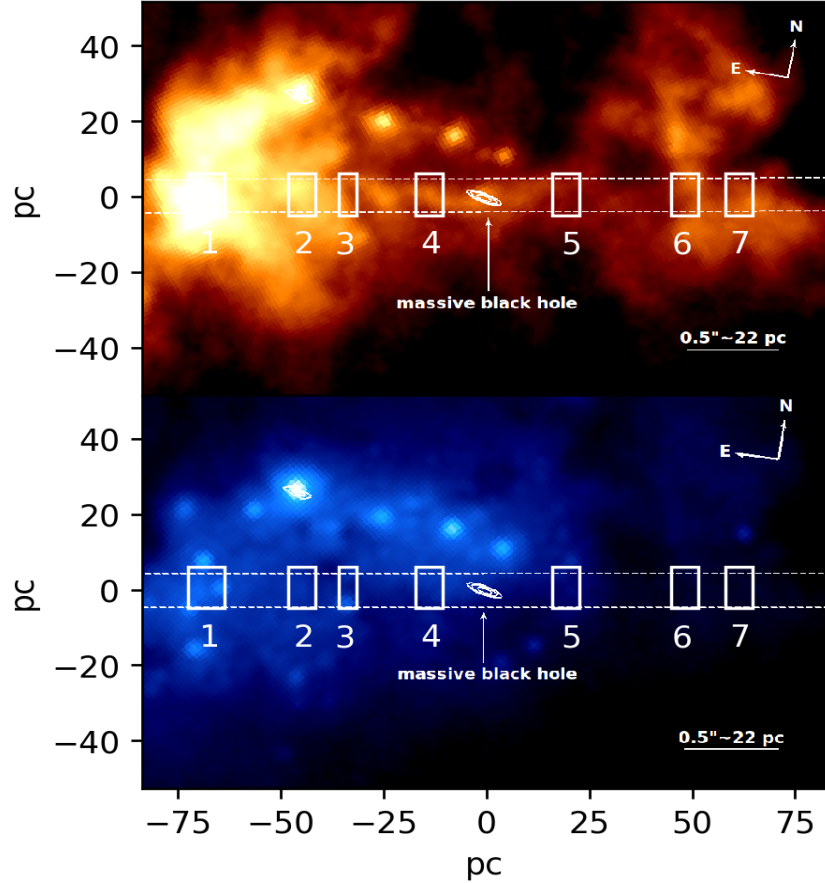


Figure 7: The spatial extraction regions taken along the EW slit orientation, which we place on optical emission line diagnostic diagrams (Figures 8-10). Top panel: the extraction regions are shown on the narrow band  $H\alpha$  + continuum image from HST to highlight the ionized gas features that several of the spatial extractions probe. Bottom panel: the extraction regions are shown on the archival 0.8 micron HST image, showing young star clusters that the EW slit orientation passes through.

We first utilize the standard emission line diagnostic diagrams described by Baldwin et al.<sup>38</sup> and Veilleux et al.<sup>39</sup> that have been expanded upon and summarized in Kewley et al.<sup>40</sup>. An accreting BH will produce a much harder continuum than is emitted by hot stars, and these diagrams take advantage of this fact by comparing strong emission line ratios that are close together in frequency to mitigate reddening effects. In this study we employ widely used emission line diagnostic diagrams that take  $[OIII]/H\beta$  versus  $[NII]/H\alpha$ ,  $[SII]/H\alpha$ , and

[OI]/H $\alpha$  (see Figure 8). In the [NII]/H $\alpha$  diagram, line-emitting galaxies separate into a V-shape<sup>40</sup> with star forming galaxies occupying the left most plume while AGNs occupy the right branch of galaxies. These regions are quantified by an empirical division between HII regions and emission from AGNs developed by Kauffmann et al.<sup>41</sup> The “composite” region between this empirical division and the theoretical maximum starburst line from Kewley et al.<sup>42</sup> indicates there is likely significant emission from both HII regions and AGNs. Like the [NII]/H $\alpha$  diagram, the [SII]/H $\alpha$  and [OI]/H $\alpha$  diagnostics provide diagnostics for differentiating between emission from HII regions and AGNs. These two diagrams add a dividing line to distinguish between emission from Seyferts and Low Ionization Nuclear Emission Regions (LINERs). LINER emission can be generated both by shocks and very hard AGN spectra and determining the primary ionization mechanism can be complicated<sup>37</sup>. It should be noted that while these diagnostic diagrams are useful for identifying regions dominated by luminous AGNs, they have limitations and can yield ambiguous results for (or completely miss) massive black holes accreting at very low Eddington ratios such as the one in Henize 2-10. Indeed, non-stellar ionization is clearly indicated in the [OI]/H $\alpha$  diagram at the location of the nuclear source, but not so for the other diagnostic diagrams (see discussion in the main paper). Figure 8 shows the [OIII]/H $\beta$  versus [NII]/H $\alpha$ , [SII]/H $\alpha$ , and [OI]/H $\alpha$  diagnostic diagrams for the various extraction regions along the EW slit.

In addition to the diagnostic diagrams discussed above, we also investigate whether the ionization conditions seen in the central regions of Henize 2-10 can be explained by mechanical excitation from shocks. To investigate this, we employ ionization models of

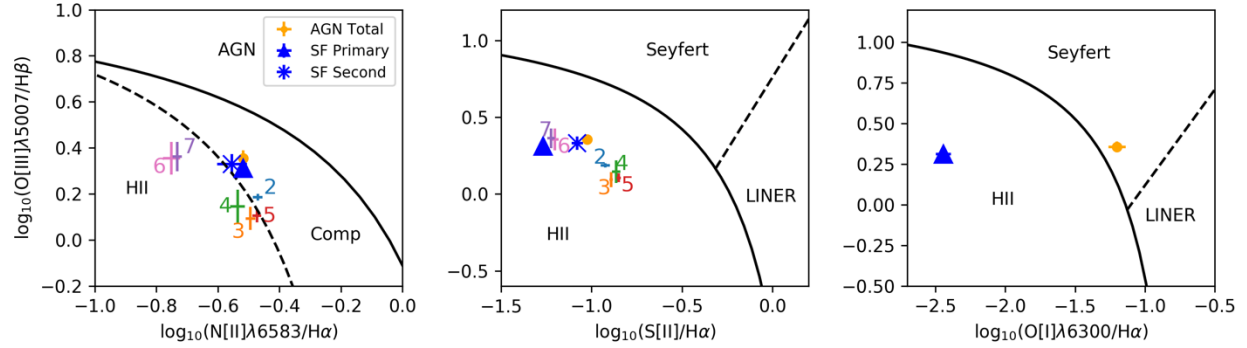


Figure 8: Narrow emission line diagnostic diagrams showing various extraction regions along the EW slit orientation (see Figure 7). The nucleus (yellow point) falls in the Seyfert region of the  $[OIII]/H\alpha$  diagram. The young star-forming region  $\sim 70$  pc to the east of the low-luminosity AGN is depicted with a blue triangle and star for the primary emission line component and the blue-shifted secondary component, respectively.  $[OI]$  is not detected in all of the regions.

shock and shock+precursor emission developed by Allen et al.<sup>25</sup>. These models provide emission line fluxes for ionization from a pure shock (possibly driven by an outflow from an AGN or by regions of intense star formation), where the gas is collisionally ionized, or a shock+precursor where ionizing photons produced in the shock-heated gas travel upstream and ionize the gas before the shock reaches it. We explore models with a variety of electron densities ( $0.01 - 1000 \text{ cm}^{-3}$ ), shock velocities (100-600 km/s) and transverse magnetic field strengths ( $0.01-32 \mu\text{G}$ ). These are shown in Figures 9 and 10.

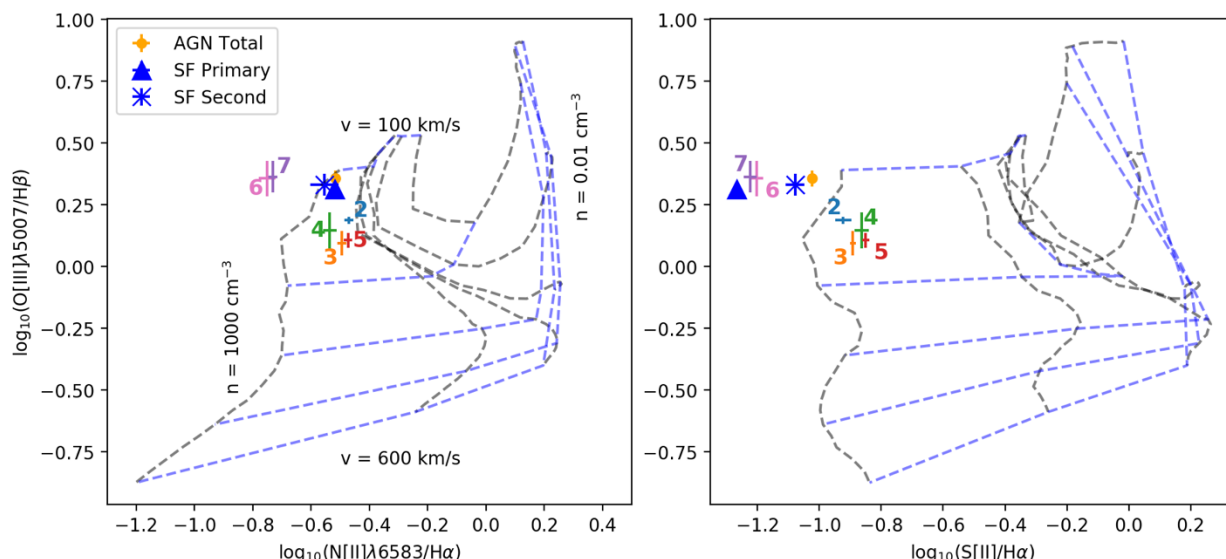
The emission line ratios from the nuclear source are best described by the shock+precursor models with a low shock velocity ( $100-250 \text{ km s}^{-1}$ ), a high-density gas ( $n = 1000 \text{ cm}^{-3}$ ), and a low transverse magnetic field parameter ( $b = 0.01 - 1 \mu\text{G}$ ) (see Figures 9 and 10). Shock+precursor models are thought to be a good description for AGN+outflow emission. Along the filament (extraction regions 2-5), the line ratios are explained well by a low velocity shock or shock+precursor model ( $\sim 200 \text{ km s}^{-1}$ ) in a high density ( $n_e \sim 1000 \text{ cm}^{-3}$ ) gas with a transverse magnetic field parameter in the range of  $1-10 \mu\text{G}$ . This is

consistent with a scenario where the central black hole is driving a bipolar outflow that shocks the gas and dominates the ionization conditions along the filament.

At the region of intense star formation located  $\sim 70$  pc to the east of the black hole, we observe strong emission lines including a secondary, blue-shifted kinematic component. To properly fit the emission lines in this region, an additional Gaussian component is added (see Figure 3 in the main paper). The separation of this component is determined using the [SII] emission line region where the secondary peak is most clearly resolved. We find that the secondary peak is offset from the primary peak by  $154 \text{ km s}^{-1}$ , and we use this value when fitting the other emission line regions where the secondary peak is not as well resolved. When comparing to shock(+ precursor) models, we find that the [NII]/H $\alpha$  diagram indicates a low shock velocity ( $100\text{-}250 \text{ km s}^{-1}$ ) in a high-density gas ( $n = 1000 \text{ cm}^{-3}$ ) with a low transverse magnetic field parameter ( $b = 0.01 - 1 \mu\text{G}$ ) (see Figures 9 and 10). The [SII]/H $\alpha$  diagram shows the primary emission peak is inconsistent with emission from shocks or shocks+precursor models. This indicates that the primary emission peak at this location is primarily due to star formation. The secondary emission peak is consistent with shock+precursor models for the low velocity, high density conditions, indicating that this kinematically distinct emission component is dominated by a shock+precursor from the AGN-driven outflow.

Emission from extraction regions 6 and 7 (i.e., the western star-forming region) is not consistent with any shock or shock+precursor models, which is in agreement with their location in the HII region of the BPT diagram. The line ratios are dominated by star formation in this region.

### Shock Models, EW Slit, $b=1\mu\text{G}$



### Shock+Precursor Models, EW Slit, $b=1\mu\text{G}$

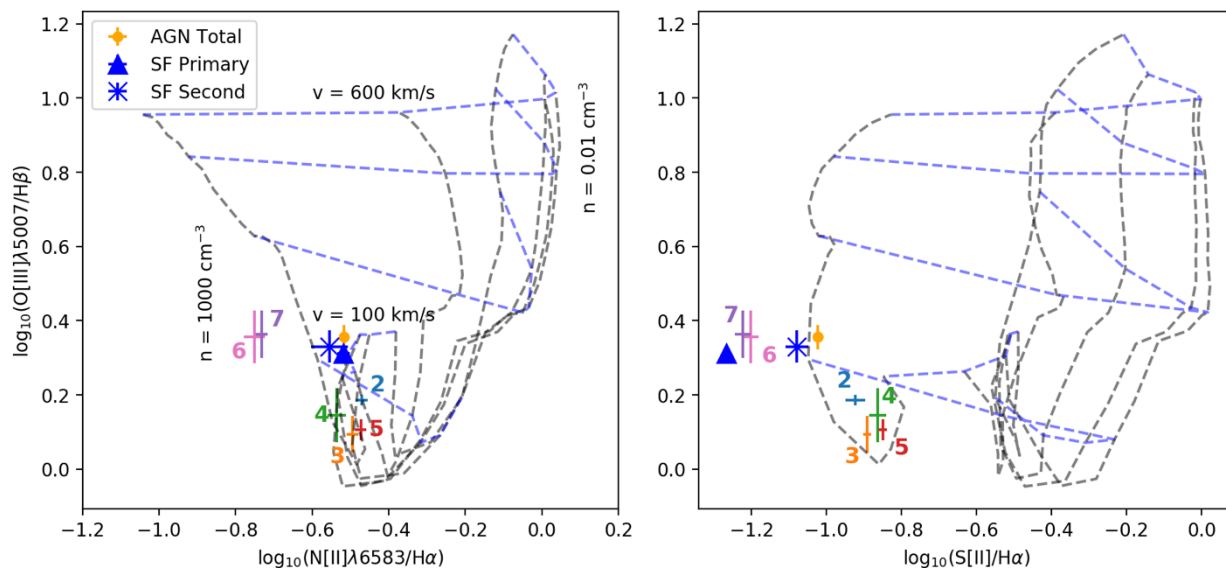
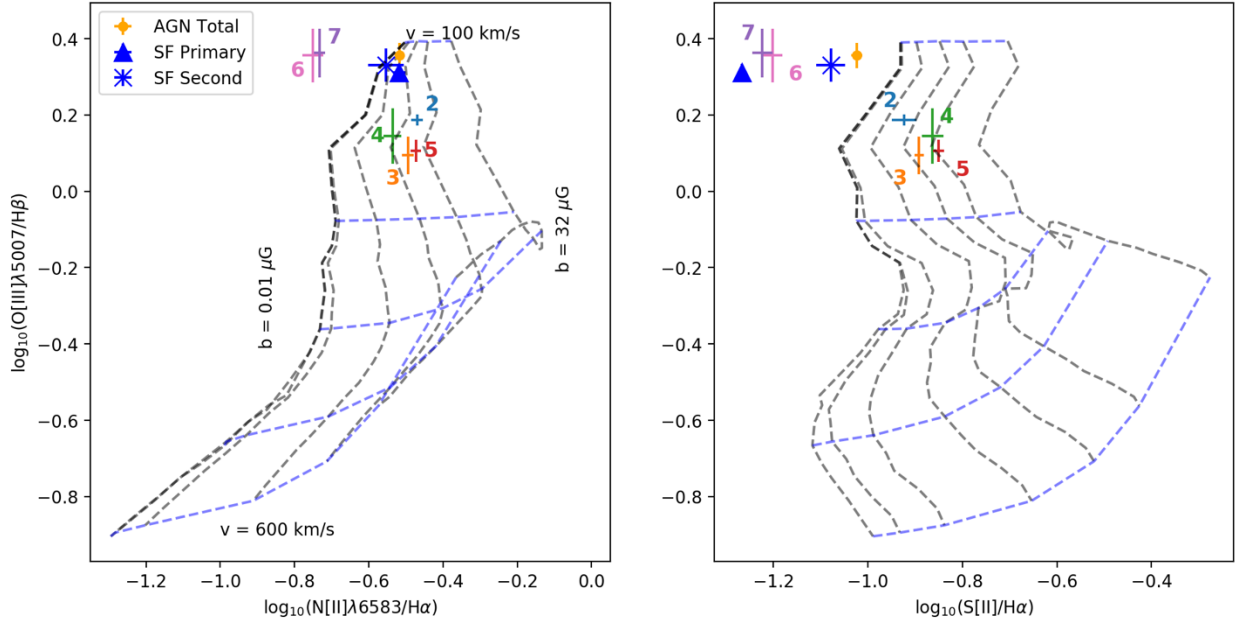


Figure 9: Optical emission line diagnostics from the shock and shock+precursor models presented in Allen et al.<sup>25</sup> We place the spatial extractions from the EW slit orientation shown in Figure 7 on a grid of shock excitation models with varying gas density ( $n = 0.01\text{-}1000\text{ cm}^{-3}$ ) and shock velocity ( $v = 100\text{-}600\text{ km/s}$ ). We fix the transverse magnetic field to be  $b = 1\mu\text{G}$  and the assume solar metallicity.

Shock Models, EW Slit,  $n=1000 \text{ cm}^{-3}$



Shock+Precursor Models, EW Slit,  $n=1000 \text{ cm}^{-3}$

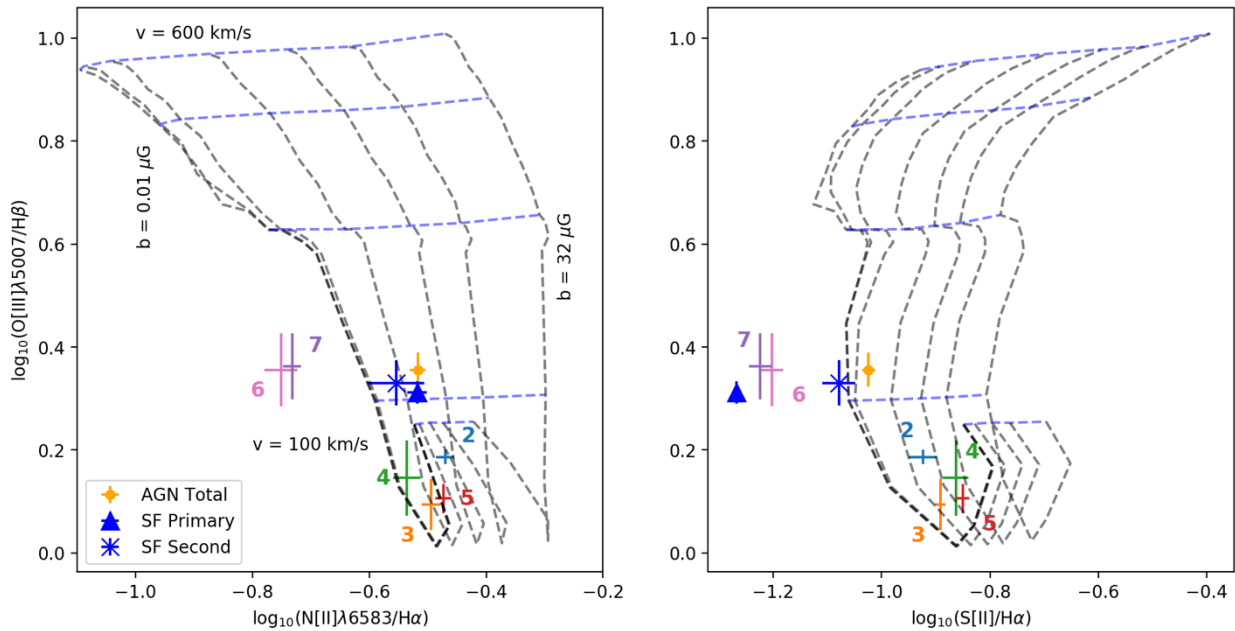


Figure 10: Optical emission line diagnostics from the shock and shock+precursor models presented in Allen et al.<sup>25</sup> The models are shown as a grid with dashed blue lines indicating constant shock velocity and dashed black lines indicating constant transverse magnetic field. For these models, the density is fixed to  $n = 1000 \text{ cm}^{-3}$  and the transverse magnetic field parameter is allowed to vary from  $b = 0.01\text{-}32 \mu\text{G}$ .

## Star Cluster Ages

We estimate the ages of the young stellar clusters that fall within the EW slit from their  $H\alpha$  and  $H\beta$  equivalent widths. To ascertain ages from these equivalent widths we employ simple stellar population (SSP) models from Starburst99<sup>35</sup>. We use models from Version 7.1 with solar metallicity (appropriate for the central regions of Henize 2-10<sup>43</sup>), an instantaneous burst of  $10^4 M_{\odot}$  with a Kroupa IMF ( $0.1 - 100 M_{\odot}$ ), the Geneva evolutionary tracks with high mass loss and the Pauldrach-Hillier atmospheres.

At the location of the young stellar clusters in the eastern star-forming region (region 1 in Figure 7) we find an equivalent width of 478 Å and 70 Å for  $H\alpha$  and  $H\beta$  respectively. These both give stellar population age estimates of  $\sim 4.3$  Myr, which is in good agreement with previous estimates of the ages of other young star clusters in the region<sup>44</sup>. The ages of these clusters are larger than the crossing time for the AGN-driven outflow ( $\sim 0.3$  Myr), based on the minimum outflow velocity measured from emission line spectra ( $\sim 200$  km/s) and the distance between the AGN and the eastern star-forming knot ( $\sim 70$  pc). Therefore, the timescales allow for the AGN-driven outflow to have triggered/enhanced the formation of star clusters in the Eastern star-forming knot.

The EW slit orientation also passes through a young star cluster in region 3. At this location we find equivalent widths of 212 Å and 41 Å for  $H\alpha$  and  $H\beta$  respectively, both indicating an age of  $\sim 5.2$  Myr for the stellar cluster. Finally, region 6 in the western star-forming region has  $H\alpha$  and  $H\beta$  equivalent widths of 1092 Å and 196 Å, respectively. These equivalent widths indicate the stellar clusters have ages  $\lesssim 3$  Myr.

## Bipolar Outflow Model

Here we provide a derivation of the model used to describe a precessing bipolar outflow emanating from the nuclear radio/X-ray source, which can explain the coherent velocity pattern seen in the central  $\sim 120$  pc of the EW orientation observations (Figure 3). In this model, we align the EW slit orientation with the  $z$ -axis and assume the outflow precesses about this axis with a small angle  $\theta$  and an angular precession frequency  $\omega$ . If the gas being ejected by the outflow has velocity  $v_0$ , and we orient the  $x$ -axis to be in the direction of the observer, then the radial (Doppler shifted) velocity seen at the location of the AGN as a function of time will be given by

$$v_r(t) = v_x(t) = v_0 \sin(\theta) \sin(\omega t + \gamma),$$

where  $\gamma$  represents a phase shift that accounts for small asymmetries in the outflow profile which are not explicitly modeled here (see Figure 11 for an illustration of our model).

To find the radial velocity as a function of distance ( $z$ ) along the slit axis, we must consider what angle the outflow made with the (line-of-sight)  $x$ -axis when the gas at distance  $z$  was emitted. Since this angle is time dependent as the outflow precesses, the line-of-sight velocity of the gas will depend on the orientation of the outflow at some time  $t_0$  in the past. The time that has passed since the gas at distance  $z$  was ejected by the outflow is determined by the  $z$  velocity of the gas. Due to the symmetry of the model about the  $z$ -axis, the  $z$  component of the gas velocity will be time independent and only depend on the angle of the outflow with the  $z$ -axis,

$$v_z = v_0 \cos(\theta).$$

The time,  $t_0$ , for gas to reach a distance  $z$  along the slit is then given by

$$t_0 = \frac{z}{v_0 \cos(\theta)}.$$

We are then able to find an expression for  $v_r(z)$  by evaluating the expression for  $v_r(t)$  at the time  $-t_0$ :

$$v_r(z) = v_0 \sin(\theta) \sin\left(\gamma - \frac{\omega}{v_0 \cos(\theta)} z\right)$$

To fit this model to the data we require a rough estimate of the bulk outflow velocity,  $v_0$ . We estimate this parameter using  $W80$ , the velocity interval containing 80% of the line flux, of the broad emission seen at the location of the candidate AGN. We find  $W80 \approx 200 - 500 \text{ km s}^{-1}$  based on measurements of the [OIII]5007 and [OI]6300 lines at the location of the candidate AGN. This allows us to determine the best-fit angle of precession,  $\theta$ , and the frequency of precession,  $f = \omega/2\pi$ , to be in the range

$$\theta = 2.4^\circ - 6.1^\circ \quad f = 3.0 - 7.5 \text{ revolutions Myr}^{-1}$$

where the larger angle of precession and smaller frequency of precession corresponds to lower outflow velocities. We find consistent results when using the Doppler shift profile of  $H\alpha$ ,  $H\beta$  and [OIII] emission lines to fit the model derived above (the results using the [OIII] emission line are shown in Figure 3). The Doppler shift profile can be coherently traced out to 50-60 pc on either side of the candidate AGN, most definitively out to the bright eastern star forming region after which the Doppler shifts of the emission lines show no coherent pattern further along the slit. The coherent velocity structure seen over 100 pc is inconsistent with a young supernova remnant as the origin of the central compact radio/x-

ray source in Henize 2-10, which provides further motivation that a low luminosity AGN is driving the outflow.

These results are roughly consistent with jet parameters derived in other studies where precessing or reorienting jet models have been applied. The long precession period we observe ( $\sim 200,000$  years) is shorter by a factor of a few than those seen predicted by Dunn et al.<sup>16</sup>, Nawaz et al.<sup>45</sup> and Cielo et al.<sup>46</sup> but longer by a factor of a few than those predicted by Gower et al.<sup>15</sup> when jet precession is invoked to explain the complex bending and knotting seen in large radio jets.

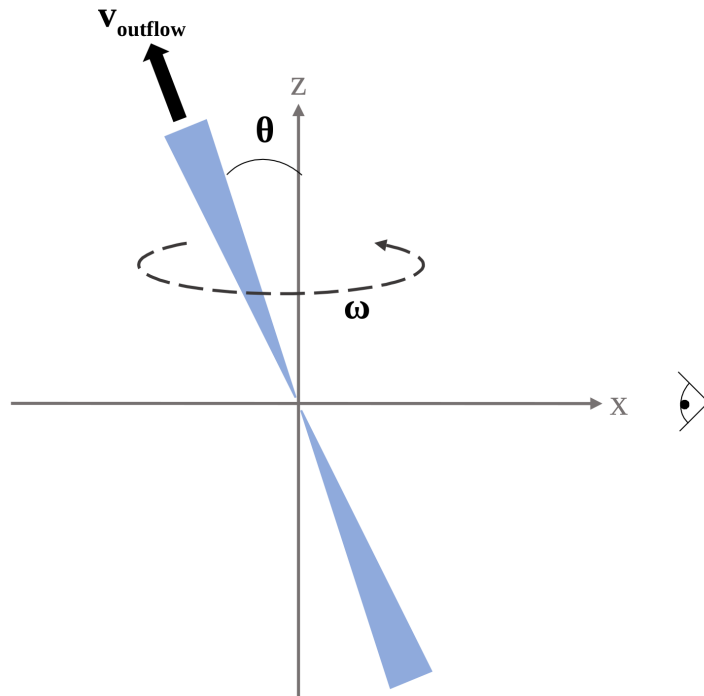


*Figure 11: A diagram of the toy model of the bipolar outflow generated by the low-luminosity AGN in Henize 2-10. Our simple model depends on the outflow velocity of the ionized gas ( $v_{\text{outflow}}$ ), the angle the outflow makes with its precession axis ( $\theta$ ) and the angular frequency with which the outflow precesses ( $\omega$ ). Similar models have been used to describe the bending seen in large radio jets<sup>15,16</sup>.*

31. Constantin, Anca, et al. "Probing the balance of AGN and star-forming activity in the local universe with ChaMP." *The Astrophysical Journal* 705.2 (2009): 1336.
32. Baganoff, Frederick K., et al. "Chandra X-ray spectroscopic imaging of Sagittarius A\* and the central parsec of the galaxy." *The Astrophysical Journal* 591.2 (2003): 891.
33. Nguyen, Dieu D., et al. "Extended structure and fate of the nucleus in Henize 2-10." *The Astrophysical Journal* 794.1 (2014): 34.
34. Greene, Jenny E., Jay Strader, and Luis C. Ho. "Intermediate-Mass Black Holes." *Annual Review of Astronomy and Astrophysics* 58 (2020): 257-312.
35. Leitherer, Claus, et al. "Starburst99: synthesis models for galaxies with active star formation." *The Astrophysical Journal Supplement Series* 123.1 (1999): 3.
36. Newville, M. Stensitzki, T., Allen, D.B. & Ingargiola, A. LMFIT: Non-Linear Least-Square Minimization and Curve-Fitting for Python version 0.8.0 Sept. 2014.  
<http://doi.org/10.5281/zenodo.11813>
37. Osterbrock, Donald E., and Gary J. Ferland. *Astrophysics Of Gas Nebulae and Active Galactic Nuclei*. University science books, 2006.
38. Baldwin, Jack A., Mark M. Phillips, and Roberto Terlevich. "Classification parameters for the emission-line spectra of extragalactic objects." *Publications of the Astronomical Society of the Pacific* 93.551 (1981): 5.
39. Veilleux, Sylvain, and Donald E. Osterbrock. "Spectral classification of emission-line galaxies." *The Astrophysical Journal Supplement Series* 63 (1987): 295-310.
40. Kewley, Lisa J., et al. "The host galaxies and classification of active galactic nuclei." *Monthly Notices of the Royal Astronomical Society* 372.3 (2006): 961-976.
41. Kauffmann, Guinevere, et al. "The host galaxies of active galactic nuclei." *Monthly Notices of the Royal Astronomical Society* 346.4 (2003): 1055-1077.

42. Kewley, Lisa J., et al. "Theoretical modeling of starburst galaxies." *The Astrophysical Journal* 556.1 (2001): 121.
43. Martín-Hernández, N. L., et al. "High spatial resolution mid-infrared spectroscopy of the starburst galaxies NGC 3256, II Zw 40 and Henize 2–10." *Astronomy & Astrophysics* 455.3 (2006): 853-870.
44. Chandar, Rupali, et al. "The stellar content of henize 2-10 from space telescope imaging spectrograph ultraviolet spectroscopy." *The Astrophysical Journal* 586.2 (2003): 939.
45. Nawaz, M. A., et al. "Jet–intracluster medium interaction in Hydra A–II. The effect of jet precession." *Monthly Notices of the Royal Astronomical Society* 458.1 (2016): 802-815.
46. Cielo, S., et al. "Feedback from reorienting AGN jets-I. Jet–ICM coupling, cavity properties and global energetics." *Astronomy & Astrophysics* 617 (2018): A58.

## Acknowledgments

We are grateful to Mallory Molina for useful discussions regarding shocks. We also thank Mark Whittle and Kelsey Johnson for their assistance with the *HST*/STIS proposal while AER was a graduate student at the University of Virginia, as well as subsequent discussions. Support for Program number HST-GO-12584.006-A was provided by NASA through a grant from the Space Telescope Science Institute, which is operated by the Association of Universities for Research in Astronomy, Incorporated, under NASA contract NAS5-26555. AER also acknowledges support for this work provided by NASA through EPSCoR grant number 80NSSC20M0231. ZS acknowledges support for this project from the Montana Space Grant Consortium.

## **Author contributions statement**

ZS reduced and analyzed the STIS data and compared the results to models. AER led the *HST/STIS* proposal and helped with the data reduction. Both authors worked on the interpretation of the results and writing of the paper.